

# A Robust Mine Detection Algorithm for Acoustic and Radar Images

Arnold Williams<sup>\*a</sup>, Rodney Meyer<sup>\*\*a</sup>, Peter Pachowicz<sup>\*\*\*b</sup>, George Maksymonko<sup>\*\*\*\*c</sup>  
<sup>a</sup>Science Applications International Corporation (SAIC); <sup>b</sup>George Mason University; <sup>c</sup>Night  
Vision and Electronic Sensors Directorate (NVESD)

## ABSTRACT

Current research in minefield detection indicates that operationally no single sensor technology will likely be capable of detecting mines/minefields in a real-time manner and at a performance level suitable for a forward maneuver unit. Minefield detection involves a particularly wide range of operating scenarios and environmental conditions, which requires deployment of complementary sensor suites such as acoustic and ground penetrating radar sensors. To aid the sensor fusion required, we have focused on the development of a computationally efficient and robust detection algorithm applicable to a variety of these imaging sensors that exploits robust image processing techniques centered on meaningful target feature sets. This paper presents the detection technique, called the Ellipse Detector, emphasizing its robust architecture, and provides performance results for image data generated by complementary sensors.

**Keywords:** mine detection, robust algorithms, ground penetrating radar imaging, acoustic imaging

## 1. INTRODUCTION

The detection and location of mines is a difficult problem that requires innovative algorithm development, including the fusion of information from complementary sensors. The Night Vision and Electronic Sensors Division (NVESD) has funded a 3-year algorithm effort as a step in solving this difficult problem. This effort began in October 2000, called the "Signal Processing and Algorithm Development for Robust Mine Detection Program" (SPAD), is being executed by SAIC with Arnold Williams as the Principal Investigator and George Maksymonko as the NVESD Contract Technical Representative.

The key word in "Signal Processing and Algorithm Development for Robust Mine Detection Program" is "robust". SPAD is developing and integrating algorithms that are built upon robust techniques. For example, we are developing a robust "Ellipse Detector" applicable to the output of a variety of imaging sensors. Such a common detector will aid robustness and fusion.

The Ellipse Detector<sup>1</sup> is a fundamental building block for our fusion approach. At present, we are considering two fusion options. One option is a decision level fusion technique<sup>2</sup> called the Piecewise Level Fusion Algorithm (PLFA). Such a technique is very robust and has been demonstrated on an earlier NVESD sponsored automatic

---

\* [awilliams@trgl.saic.com](mailto:awilliams@trgl.saic.com); phone: 1 407 331 3146; fax: 1 407 331 8740 ; SAIC, 444 Golfview Dr., Longwood, FL 32750

\*\* [rodney.p.meyer@saic.com](mailto:rodney.p.meyer@saic.com); phone: 1 703 248 7712; fax: 1 703 522 6006; SAIC, 4001 North Fairfax Blvd., Suite 450, Arlington, VA 22203

\*\*\* [ppach@gmu.edu](mailto:ppach@gmu.edu); phone: 1 703 993 1552; fax: 1 703 993 1601; Dept. of Electrical and Computer Engineering, George Mason University, 4400 University Dr., Fairfax, VA 22030;

\*\*\*\* [george.maksymonko@nvl.army.mil](mailto:george.maksymonko@nvl.army.mil); phone: 1 703 704 2420; fax: 1 703 704 1490; NVESD, AMSEL-RD-NV-CSD-MD, Bldg. 307, Suite 121B, Ft. Belvoir, VA 20660-5806

<sup>1</sup> N. Bennett, R. Burrige, and N. Sato, "A Method to Detect and Characterize Ellipses Using the Hough Transform", *IEEE Trans. PAMI*, Vol. 21, No. 7, July, 1999, pp.652-657

<sup>2</sup> S. Thomopoulos, et. al., "Optimal Decision Fusion in Multiple Sensor Systems", *IEEE Trans. AES*, vol. AES-23, no. 5, Sept. 1987, pp.644-653

## Report Documentation Page

|   |  |  |
|---|--|--|
| <b>Report Date</b><br>00 Oct 2000   | <b>Report Type</b><br>N/A                          | <b>Dates Covered (from... to)</b><br>-       |
| <b>Title and Subtitle</b><br>A Robust Mine Detection Algorithm for Acoustic and Radar Images  |  | <b>Contract Number</b>                       |
|   |  | <b>Grant Number</b>                          |
|   |  | <b>Program Element Number</b>                |
| <b>Author(s)</b>  |  | <b>Project Number</b>                        |
|   |  | <b>Task Number</b>                           |
|   |  | <b>Work Unit Number</b>                      |
| <b>Performing Organization Name(s) and Address(es)</b><br>Science Applications International Corporation (SAIC) 4001<br>North Fairfax Blvd Suite 450 Arlington, VA 22203  |  | <b>Performing Organization Report Number</b> |
| <b>Sponsoring/Monitoring Agency Name(s) and Address(es)</b><br>Department of the Army, CECOM RDEC Night Vision &<br>Electronic Sensors Directorate AMSEL-RD-NV-D 10221<br>Burbeck Road Ft. Belvoir, VA 22060-5806   |  | <b>Sponsor/Monitor's Acronym(s)</b>          |
|   |  | <b>Sponsor/Monitor's Report Number(s)</b>    |
| <b>Distribution/Availability Statement</b><br>Approved for public release, distribution unlimited   |  |  |
| <b>Supplementary Notes</b><br>See also ADM201471, Papers from the Meeting of the MSS Specialty Group on Battlefield Acoustic and Seismic Sensing, Magnetic and Electric Field Sensors (2001) Held in Applied Physics Lab, Johns Hopkins Univ, Laurel, MD on 24-26 Oct 2001. Volume 2 (Also includes 1999 and 2000 Meetings), The original document contains color images. |  |  |
| <b>Abstract</b>   |  |  |
| <b>Subject Terms</b>  |  |  |
| <b>Report Classification</b><br>unclassified  | <b>Classification of this page</b><br>unclassified |  |
| <b>Classification of Abstract</b><br>unclassified   | <b>Limitation of Abstract</b><br>UU                |  |
| <b>Number of Pages</b><br>14  |  |  |

target recognition (ATR) program for vehicle detection and recognition.<sup>3</sup> Our second option is to consider pixel level fusion, which is ably supported by the Ellipse Detector since it accurately estimates the ellipse center of the detected object. These centers can be exploited to register the pixels from images of diverse sensors, thereby, aiding pixel level fusion.

Another aspect of robustness to be addressed by SPAD is to develop a method that adapts the detection and fusion parameters to the changing situation and environment. The inability of current ATR algorithms to adapt has been a major problem, resulting in non-robust systems that, at best, perform well on inputs similar to the training data but otherwise fail. We will use a technique called "model evolution"<sup>4</sup> to implement adaptive algorithms. This technique has been developed over several years and has been demonstrated for detecting vehicular targets in a system called IA-Chameleon.<sup>5</sup>

The SPAD effort is embodied in a hypothetical integrated detection algorithm shown in Figure 1. SPAD would be overly ambitious except that substantial software tools and proven ATR technologies are already available as shown in Figure 2.

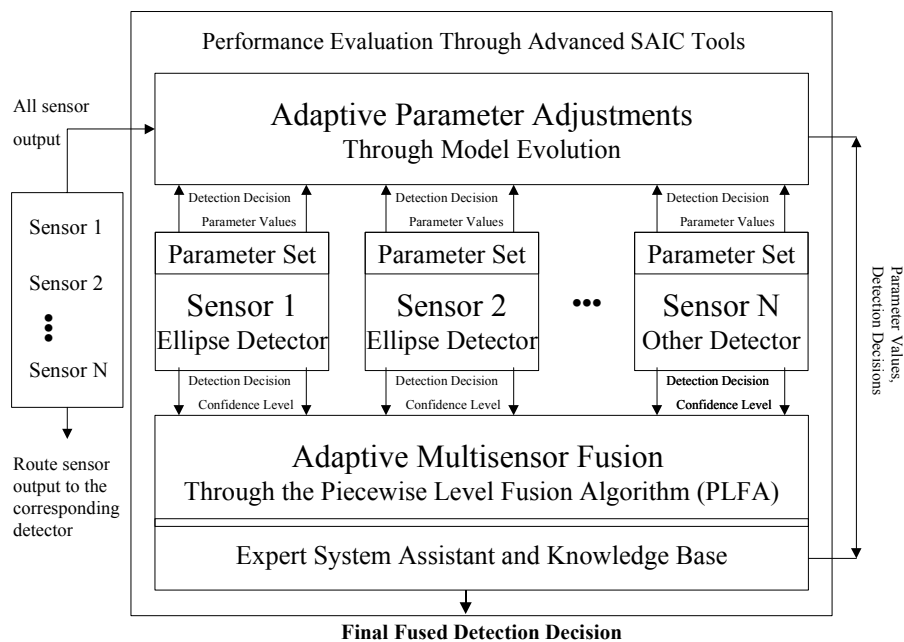


**Figure 1 Architecture of the robust detection algorithm**

| Benefits Provided  | Technologies To Be Further Demonstrated  |
|--|--|
| The fundamental detection technique will be robust and easily computed.  | The Ellipse Detector is robust and is based on affine geometry, Canny edge detection, and Hough transforms as demonstrated on an NVL mine hunting SBIR and on SAR ground target detection. |
| The fundamental detection technique will be integrated with an efficient adaptive technique that allows for changing scenarios and environments. | The Ellipse Detector has a small well-defined set of parameters amenable to adaptive techniques that will be adapted through "model evolution" as demonstrated on the IA-Chameleon system. |

<sup>3</sup> R. Patton, A. Williams, et al., "Stationary Target Detection/Identification Using MMW Genetic Algorithms and MMW/FLIR Piecewise Level Classification Fusion", *5th ATR System and Technology Symposium*, 23-25 July 1996

<sup>4</sup> L. Goldfarb, "On the Foundation of Intelligent Processes - I. An Evolving Model for Pattern Learning," *Pattern Recognition*, Vol.23, No.6, 1990, pp.595-616

<sup>5</sup> P. Pachowicz and A. Williams, "IA-CHAMELEON: A SAR Wide Area Image Analysis Aid," *Proc. ATRWG Workshop*, Baltimore, MD, July 1996

|   |   |
|---|---|
| The adaptive detection algorithm will allow fusion through multiple sensors or multiple looks of the same sensor.                           | The Ellipse Detector has performed well for different sensors and applications. It is, therefore, an ideal fusion building block. The Piecewise Level Fusion Algorithm (PLFA) easily interfaces with different detection algorithms as demonstrated on an NVL SBIR where FLIR detector decisions and radar detector decisions were fused. |
| The fusion technique, itself, will be adaptable to changing scenarios and environments.   | SAIC has developed an adaptive PLFA fusion technique by exploiting knowledge based systems technology as demonstrated on an Army Research Lab (ARL) SBIR.   |
| Techniques for evaluating algorithm performance and the performance of their feature sets will be exploited to speed algorithm development. | We have previously developed many performance evaluation tools and techniques that analyze multidimensional data and estimate the Bayes error and other performance metrics, providing useful insights on NVL and many other data sets.   |

**Figure 2 Component technologies used in the development of the mine detection algorithm**

The following sections focus on the development and results for our Ellipse Detector. We point out the robust nature of this technique in order to indicate our current progress in building a robust mine detection algorithm applicable to a wide variety of imaging sensors.

## 2. ELLIPSE DETECTOR STRUCTURE

A key element in our approach to robust mine detection is the development of a detector applicable to a variety of imaging sensors. Figure 3 presents the Ellipse Detector and points out its robustness and wide applicability.

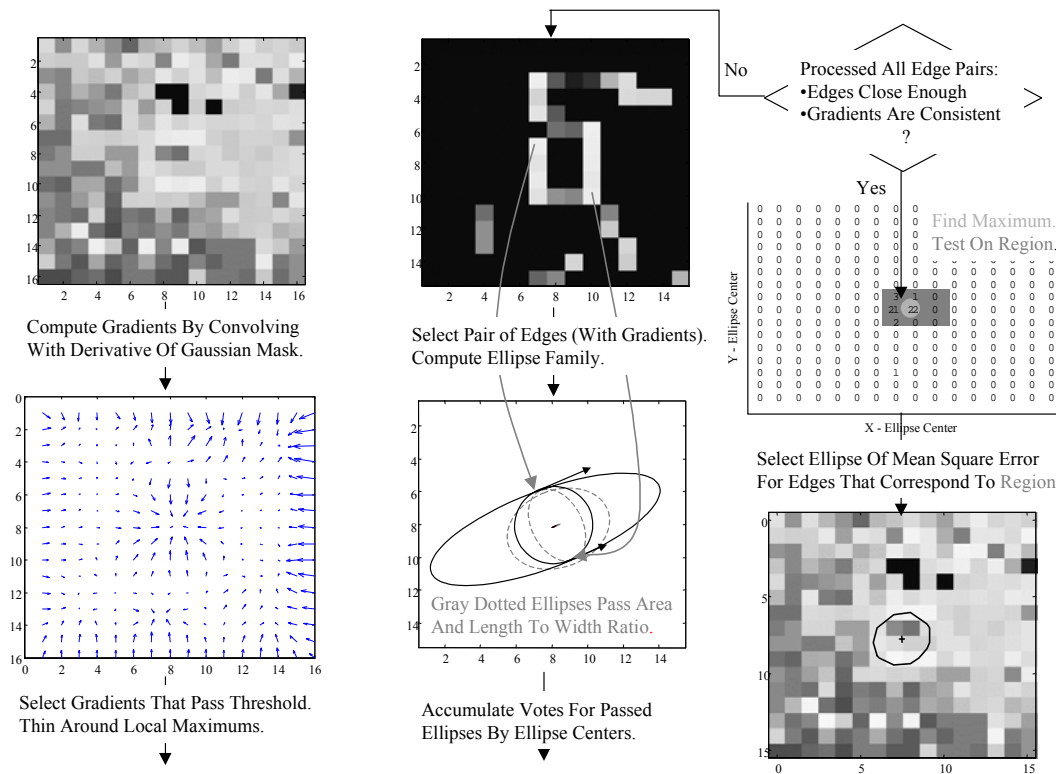


**Figure 3 The Ellipse Detector exploits a Canny edge detector and a Hough transform with *a priori* physical constraints of the mine for robust detection of the mine boundary and center.**

The following steps summarize the Ellipse Detector:

1. Edge detection: The Canny edge detector<sup>6</sup> is used to extract mine edges. The Canny method finds edges by convolving the image with the first order derivative of a 2-D Gaussian mask. This produces a set of pixels and their gradients that lie on the edges of objects within the image as illustrated in the left lower panel of Figure 3.
2. Ellipse fitting: This pairwise fitting is done for every two pixels on the edge. Use the pixel locations and the derivative information (the directions of the normal) to fit ellipses that pass through the two pixels as shown in the center panels of Figure 3. That is, each pair of pixels and their gradients generate a family of ellipses that pass through the pixel pair and are tangent to the normals of the gradients.
3. Ellipse detection: Find eligible ellipses from the family based on prior information related to mine shapes and mine sizes. Construct a "hit table" based on the Hough Transform<sup>7</sup> for these eligible ellipses. This eligibility is based on ellipse size (area should be within prescribed bounds and center should lie inside the image) and parameters (ratio of major and minor axis should be within prescribed bounds) as shown in the upper right panel of Figure 3.
4. Mine location approximation: If the hit table of the Hough Transform satisfies the condition that the total number of hits and the percentages of hits in a region exceed some thresholds, a mine is detected. An bounding ellipse from the eligible ellipses is then selected and drawn that is the best fit to all the edges within the detection region as shown in the lower right panel of Figure 3.

The ellipse detection method has the following advantages:

1. Robustness: The ellipse detection method is robust since minimal information is required from the data. Sophisticated feature extraction tools and techniques such as segmentation are not necessary. The detector is not dependent on complete or smooth edges but only on pairwise roughly oriented pixels. One of the main drawbacks with many edge-based methods is that they fail when edges are fragmented, spurious, and missing due to clutter and obscuration. Since the Ellipse Detector accumulates information by a pairwise evaluation of pixels, it is robust with respect to the effects of clutter and obscuration.
2. Pixels on Target: Resolution is a great concern when working with images. Many image detection techniques can require on the order of 50 - 100 pixels on target or even more if well defined boundaries are required. One advantage of the Ellipse Detector is that it appears to work well even with as few as 8 pixels on target. For example, the

pairwise nature of the algorithm allows 8 pixels to cast as many as  $\binom{8}{2} = 28$  detection votes in the hit table.

3. Implicit fusion across spectral bands: Fusing information across spectral bands has many challenges such as the alignment and registration of the imagery. One of the advantages of our method is that it implicitly fuses and accumulates the ellipse information across spectral bands. When the Canny edge detector is applied to a spatial image for each frequency band, the hit table can accumulate this evidence across all the images. That is, steps 1 through 3 of the Ellipse Detector that follows Figure 3 are repeated for each image, accumulating the hits in the hit table. Step 4 (the final detection decision) is then performed after all images have been processed. Thus, ellipse fitting can be done across spectral bands (images) through an implicit integration of pixel detections, allowing a seamless method of combining information across spectral bands.

### 3. ELLIPSE DETECTOR DEVELOPMENT

The Ellipse Detector is being successfully developed and tested on several sensors. The anecdotal results in this section illustrate the development and operation of the Ellipse Detector. While these results are anecdotal because of the limited sample size, the robustness of the detector is indicated due to its uniformly good results over a variety of sensors and images. We have found the Ellipse Detector effective on acoustic mine images produced by the University of Mississippi Laser Doppler Vibrometer (LDV)<sup>8</sup>, on radar mine images produced by the Planning

---

<sup>6</sup> M. Yi, J. Koo, "Basic Image Processing Demos (for EECS20)", 6 April, 1996, <http://eclair.eecs.berkeley.edu/~mayi/imgproc/index.html>

<sup>7</sup> A. Rosenfeld and A. Kak, *Digital Picture Processing, Volume 2*, Second Edition, pp. 121-126, Academic Press, Orlando, FL, 1982

<sup>8</sup> J. Sabatier and N. Xiang, "Acoustic Technology for Mine Detection", Progress, Status and Management Report, National Center for Physical Acoustics, University of Mississippi, University, Mississippi 38677, September 15, 1998

Systems Incorporated (PSI) Ground Penetrating Radar (GPR)<sup>9</sup>, and on synthetic aperture radar (SAR) images of adjacent vehicular targets<sup>10</sup>.

Figure 4 typifies Ellipse Detector results on tens of LDV Images. The detector has been able to reliably detect most mines with practically no false alarms. The edges found by the Canny edge detector are usually strong and form a boundary of the mine when it exists. Such bounding pixels do not generally exist for clutter only images. The LDV produces a down range/cross range image for a number of spectral bands. The "Raw Images" in Figure 4 are noncoherent sums of these images on a pixel basis over the entire spectral band from 80 to 300 Hz.

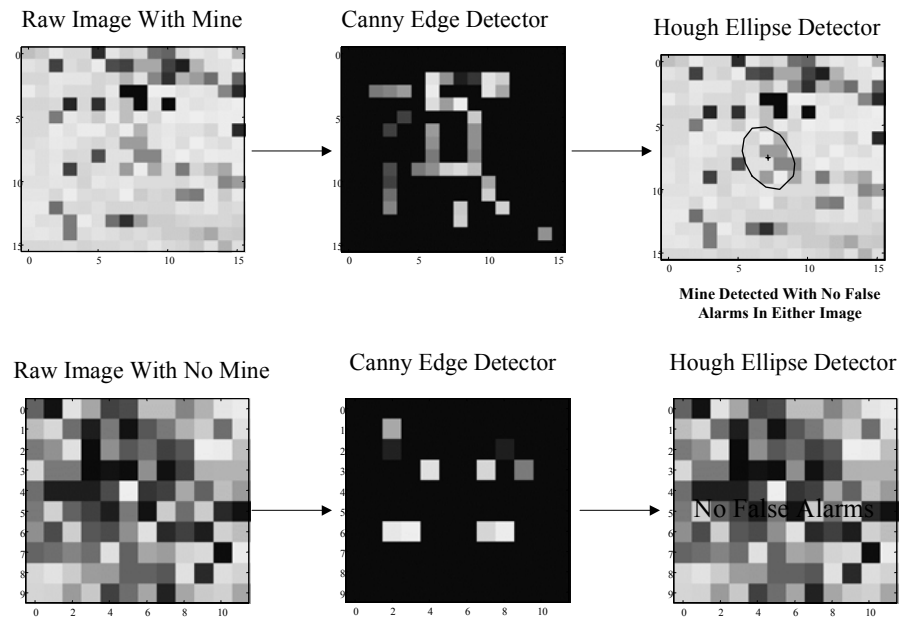


**Figure 4 Typical Ellipse Detector results on LDV images**

As indicated in item 3 above of the "Ellipse Detector advantages" list, we have developed an Ellipse Detector that accumulates evidence over the individual spectral images and then makes a detection decision. This Ellipse Detector outputs the optimal spectral band for the detected mine from these collection of images as well as the bounding ellipse and ellipse center. Figure 5 illustrates the 3-D hit table, i.e., the 2-D table with an additional frequency dimension, and shows a typical output where the image is noncoherently summed only over the (115,140) Hz subband. This image is much improved relative to the image over the entire (60,300) Hz band shown in the bottom left image of Figure 9.

<sup>9</sup> M. Bradley, M. Duncan, and R. McCumms, "GPR Processing Software -- User Guidelines", Planning Systems Incorporated, Long Beach, Mississippi, June 1999

<sup>10</sup> E. R. Keydel, S.W. Lee, and J.T. Moore, "MSTAR extended operating conditions: a tutorial", *Proc SPIE*, Vol. 2757, pp.228-242, Algorithms for synthetic Aperture Radar Imagery IV, April 1997

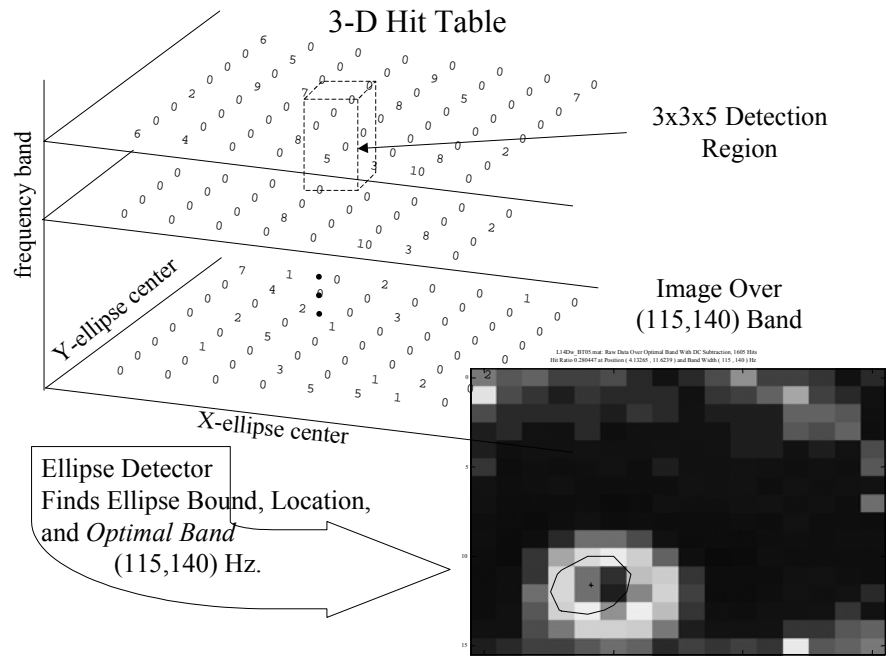


**Figure 5 The Ellipse Detector fuses over the LDV frequency band to find the mine.**

We have also examined the Ellipse Detector over tens of GPR images. The GPR produces 3-D images as a function of range, cross range, and depth. We currently work with only 2-D GPR images produced by taking the maximum value with respect to depth over each pixel. A typical result is shown in Figure 6. Note that the mine is detected and that the hot spots visible to the left and the top right in the raw mine image have been correctly ignored due to their non-mine like spatial characteristics. Also note that, correctly, no mine (false alarm) is found in the bottom clutter image sequence of the figure.

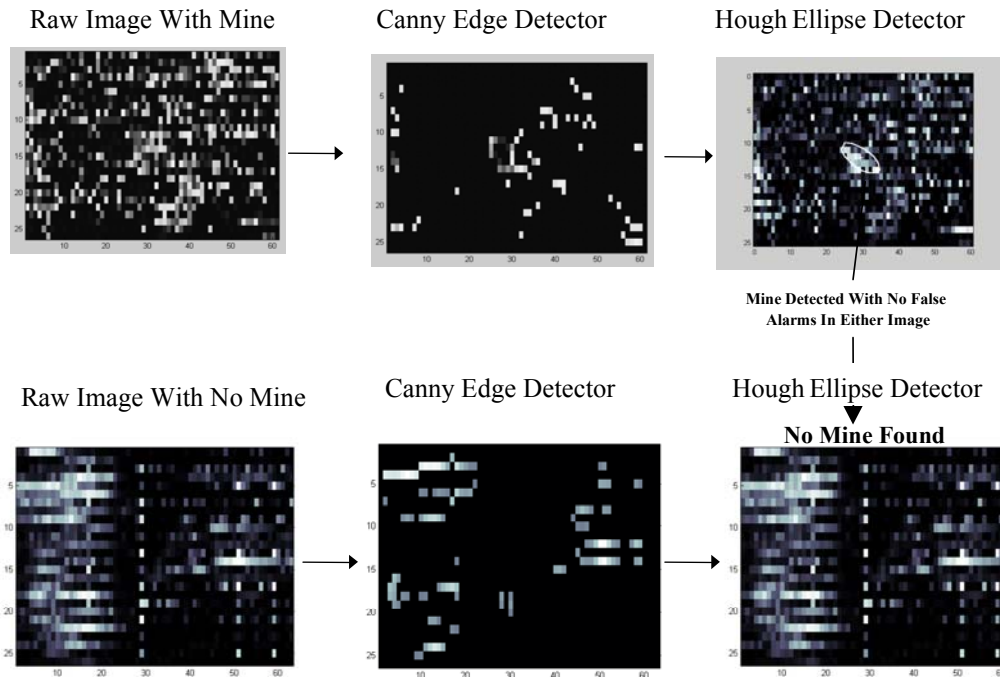


**Figure 6 Typical Ellipse Detector results on GPR images**

The Ellipse Detector has also been applied to the two SAR images shown in Figure 7, each containing two adjacent vehicular targets<sup>11</sup>. As shown in Figure 8, three of the four targets were correctly detected. Note that in the bottom right image of Figure 8 the T62 was missed and the M60 was found instead. The particular orientation of the T62 in the image produces only a few weak pixels so the missed detection is not surprising.

As in the previous cases discussed above for the LDV and GPR sensors, the Ellipse Detector algorithm itself was not changed. Only the parameters that reflect the physical target sizes were changed. The two tables in Figure 7 illustrate the physical target characteristics and the derived parameter values used by the Ellipse Detector.

Automatically detecting adjacent targets in SAR images is known to be a very difficult task. The good Ellipse Detector performance, despite this limited SAR data set, is especially gratifying since the algorithm developed for one application has been successfully applied with minimal changes to a completely different application.

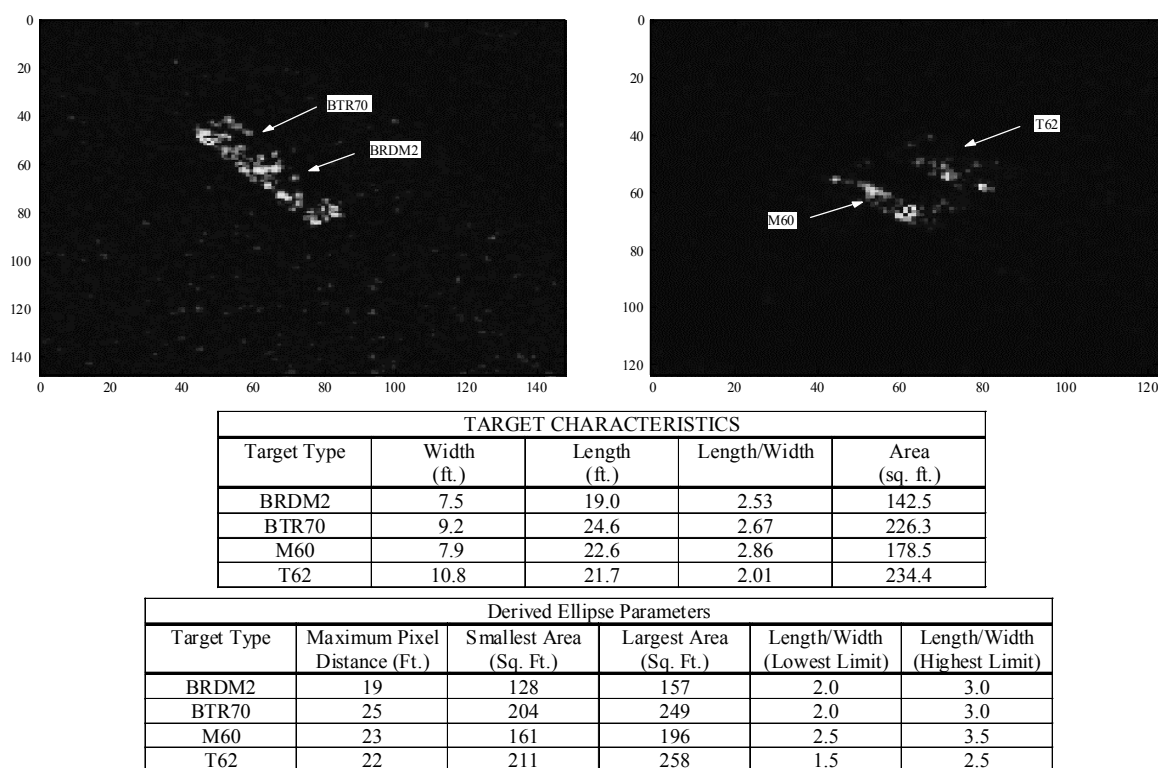


**Figure 7 Adjacent vehicular targets in SAR images**

<sup>11</sup> A. Williams, "Mine Detection and SAR Target Detection (Determining Algorithm Robustness)", viewgraph presentation, presented at SAIP IPT, 23 May 2000

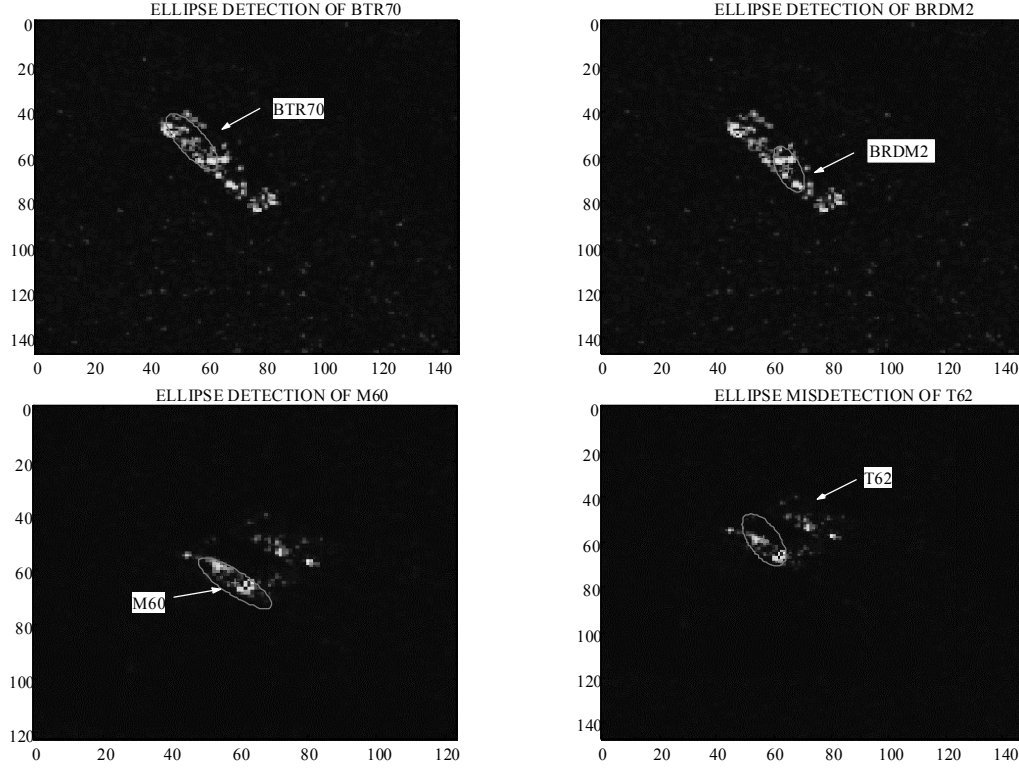


**Figure 8 Ellipse Detector results on adjacent vehicular targets in SAR images**

#### **4. SIGNAL PROCESSING TECHNIQUES AND RESULTS**

We have found that some signal processing on the raw LDV and GPR sensor outputs improves image quality and, thereby, aids detection. This signal processing is most effective and robust if it directly exploits the physics of the sensor, background, and target phenomenologies. Since these phenomenologies are only interpretable as perceived through the sensors, this signal processing is inherently sensor dependent. These observations are generally true for all ATR systems. In this section, we describe some physics based pre-detection signal processing found useful for first the LDV data and then the GPR data.

This pre-detection signal processing is implemented as predetectors in front of the Ellipse Detectors in Figure 1. Our current experimentation and past ATR experience indicates that these predetectors must be sensor dependent. The structure and actual signal processing required also depends on the Ellipse Detector needs. We anticipate, however, that the sensor dependent signal processing required will be minimized due to the robustness of the Ellipse Detector.

Figure 9 shows the need for DC correction and provides an example of its benefit on image quality. The top three plots in the figure represent mine data for three mines that have been visually characterized as good, fair, and bad, depending on the ability of a trained human to detect the mine. The horizontal axis represents the pixel position of a 16x16 LDV image for a given frequency arranged in row order. The vertical axis represents the 21 frequencies (46 for the Fair Mine) at which the image data was taken. That is, each plot has columns of signal strength (lighter is stronger) for a particular pixel over 21 (or 46) frequencies and rows of signal strength for a row-organized image at a particular frequency.

The top left plot (Good Mine) shows the structure expected for a mine since it is spatially compact and exhibits some frequency selectivity. We should expect to see a few strong well defined, reasonably adjacent, segmented columns, corresponding to the spatially adjacent mine pixels with the segments indicating good frequency bands. As we proceed from Good Mine to Bad Mine, we see an increase in obscuring signal across an entire row whose strength varies from row to row.

The LDV generates a complex signal at each frequency and pixel. By computing a complex mean across each row, we observe non-zero "DC terms" where the obscuration occurs. When these DC terms are subtracted row by row from the complex pixels, improved images generally result for each frequency. The two bottom images of Figure 9 illustrate this improvement combined with the ability of the Ellipse Detector to select an optimal frequency subband for image formation. The improvement here is demonstrated on a mine data set that would be visually classified as between good and fair so the improvement is not as dramatic as on some of the poorer data sets. Nevertheless, improved image quality is apparent.

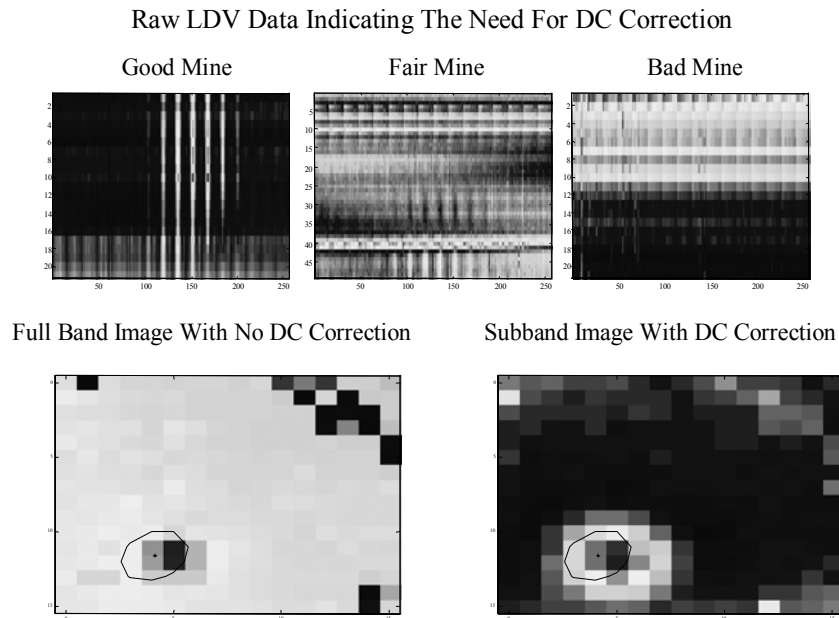


**Figure 9 Image processing and subband image formation improves LDV image quality.**

The PSI GPR sensor is composed of 26 alternating antenna pairs in two banks. The antenna pairs in the two banks are offset by a half pixel cross-track. Since this GPR is a stepped frequency system, the initial data processing step is a Fourier transform that transforms the data into three-dimensional voxels of complex numbers. That is, cross range sampling is provided by the antenna spacing, down range sampling by the forward motion of the system, and depth sampling by the Fourier transform output. Taking the maximum strength depth sample at each range/cross range pixel creates the top view image. The top row of Figure 10 shows that generating interpretable top view images requires signal processing before the Ellipse Detector is successfully employed as shown in the corresponding processed images in the bottom row.

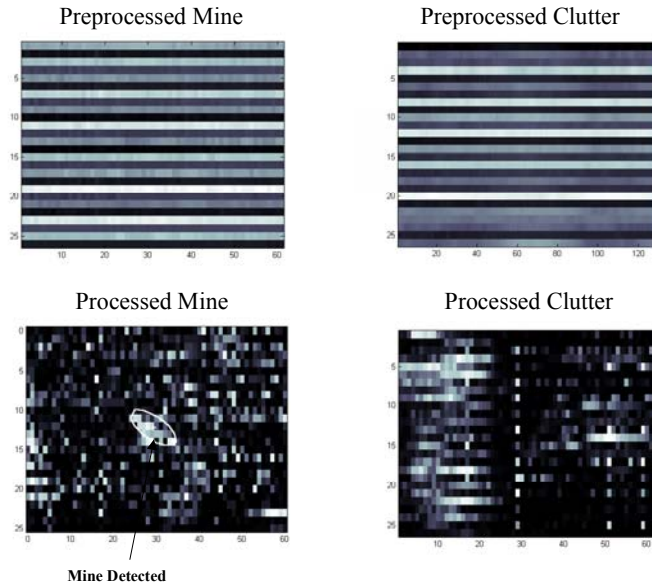


**Figure 10 Raw PSI GPR output requires signal processing before mine detection.**

Our GPR signal processing that produces an interpretable image for the Ellipse Detector proceeds in several steps as illustrated by the images in Figure 11. All images are created by plotting the maximum strength sample at any depth in the down range/cross range positions. The top two images are the front and back normalized images produced separately from the two array banks. For each antenna pair, the normalization begins by computing the median strength along the line of motion for each depth. For each sample, the appropriate median is subtracted from the sample strength for the appropriate antenna and depth, which is then divided by the square root of this median.

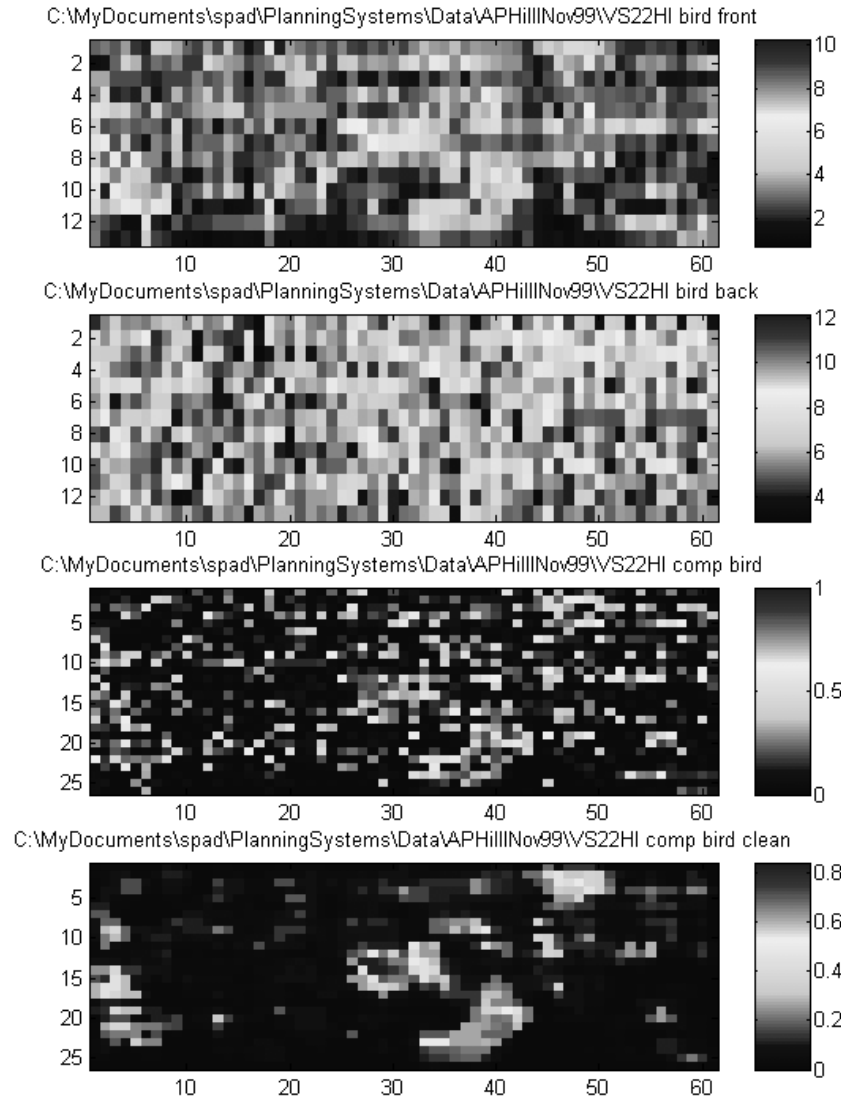


**Figure 11 GPR signal processing applied to improve image quality for Ellipse Detector input and human inspection.**

The normalized front and back images are seamlessly merged, using hyperbolic histogram equalization<sup>12</sup>, shown in the third image. This merging doubles the number of pixels on target over an individual front or back image. We found that the pixels surrounding the target could also be extracted from the noise. This allowed for even more pixels on target and better ellipse detection. Some images became very easy to detect using this method.

The fourth image is the result of further processing on the third image to reduce salt-and-pepper noise for improved human inspection. The salt-and-pepper noise has been removed by using 2-D median filtering<sup>13</sup>. The Ellipse Detector is relatively immune to such salt-and-pepper noise, so both image 3 and image 4 are equally good inputs to the Ellipse Detector. The removal of this noise does, however, aid human detection. Note that the Ellipse Detector guided by mine spatial characteristics correctly ignores the hot spots to the left and the top right of the fourth image.

<sup>12</sup> W. Frei, "Image enhancement by histogram hyperbolization", *Comput. Graphics Image Processing*, **6**, 1997, pp. 286-294

<sup>13</sup> A. Rosenfeld and A. Kak, *Digital Picture Processing, Volume 1*, Second Edition, pp. 261-264, Academic Press, Orlando, FL, 1982

This Ellipse Detector result, i.e., the ellipse bounding the mine, is shown in the top right most image of Figure 6, which is the same image as the third image of Figure 11.

## 5. ELLIPSE DETECTOR PERFORMANCE VERSES HUMAN PERFORMANCE

The Institute for Defense Analysis (IDA) has designed a blind test procedure and has performed an independent performance assessment of both the University of Mississippi (UM) Laser Doppler Vibrometer (LDV) and the Planning System Incorporated (PSI) Ground Penetrating Radar (GPR) sensors. A general description of the blind test procedure along with LDV test results are given in a paper<sup>14</sup> and the results of the assessment based upon ground truth for both the LDV and GPR are summarized in some detail in an IDA table<sup>15</sup>

The purpose of the IDA blind test was to assess the performance of the sensors themselves under human expert control. No automatic target recognizers (ATRs) were used during the blind test. The detection results for the blind test are summarized as  $P_D = 0.95$  at  $P_{FA} = 0.03$  for the LDV and  $P_D = 0.76$  at  $P_{FA} = 0.03$  for the GPR. These results were obtained in the field at near real time with human involvement and human decision making. Some of this human involvement included exploiting various data displays and alternative sensor resolution based upon human judgement as permitted by the previously specified IDA procedure. Neither UM nor PSI knew the ground truth of the test site at the time that the blind tests were being conducted.

In this section, we give the Ellipse Detector results in comparison to the UM and PSI blind test results obtained by IDA. At the time we obtained our Ellipse Detector results, we did not have the ground truth from the IDA table that we later used for scoring. The Ellipse Detector parameter values, fixed during our test, have been previously obtained on data different than the blind test data.

Figure 12 shows the Ellipse Detector (ED) results on the 59 files (19 target files and 40 clutter files) used during the IDA blind tests on the LDV sensor.

| TestSetApr99 Directory |    |      |   |         |    |     |   |          |    |     |   |
|------------------------|----|------|---|---------|----|-----|---|----------|----|-----|---|
| L03_002                | 67 | 1543 | M | L03_020 | 25 | 382 | C | L04_023  | 13 | 180 | C |
| L03_004                | 65 | 1247 | M | L03_010 | 25 | 285 | C | L04_011  | 13 | 197 | C |
| L03_005                | 62 | 1365 | M | L04_019 | 24 | 263 | C | L03_024  | 13 | 239 | C |
| L04_021                | 61 | 1168 | M | L03_015 | 23 | 244 | C | L04_024  | 12 | 358 | M |
| L04_020                | 57 | 1173 | M | L04_015 | 22 | 222 | C | L04_001  | 12 | 227 | C |
| L04_006                | 52 | 942  | M | L03_014 | 22 | 310 | C | L02_001  | 11 | 226 | C |
| L04_003                | 51 | 801  | M | L03_023 | 20 | 357 | C | L04_026  | 10 | 167 | C |
| L04_007                | 50 | 807  | M | L03_012 | 20 | 422 | C | L04_005  | 10 | 54  | C |
| L03_017                | 50 | 1047 | M | L02_002 | 19 | 275 | C | L04_004  | 10 | 158 | C |
| L03_013                | 48 | 663  | M | L03_021 | 18 | 211 | C | L03_019  | 10 | 198 | C |
| L04_025                | 42 | 789  | M | L04_018 | 17 | 206 | C | L03_007  | 10 | 215 | C |
| L03_022                | 41 | 710  | M | L03_028 | 17 | 367 | C | L03_001B | 10 | 151 | C |
| L04_009                | 37 | 668  | M | L04_022 | 16 | 209 | C | L04_014  | 8  | 178 | C |
| L03_027                | 37 | 419  | M | L03_011 | 16 | 203 | C | L04_010  | 8  | 264 | C |
| L04_012                | 33 | 334  | M | L05_002 | 15 | 195 | C | L02_003  | 8  | 164 | C |
| L03_025                | 33 | 381  | M | L04_017 | 15 | 189 | C | L04_016  | 6  | 210 | C |
| L03_018                | 31 | 502  | M | L03_006 | 15 | 221 | C | L03_026  | 6  | 189 | C |
| L04_013                | 30 | 657  | M | L04_008 | 14 | 203 | C | L03_016  | 2  | 174 | C |
| L03_009                | 26 | 361  | M | L04_002 | 14 | 259 | C | L03_003  | 2  | 327 | C |
| L05_001                | 25 | 307  | C | L03_008 | 14 | 133 | C |          |    |     |   |

██ denotes misdetection

██ denotes false alarm

**Figure 12 Ellipse Detector performance on LDV blind test set**

<sup>14</sup> E. Rosen, K. Sherbondy, and J. Sabatier, "Performance Assessment of a Blind Test Using the University of Mississippi's Acoustic/Seismic Laser Doppler Vibrometer (LDV) Mine Detection Apparatus at Fort A. P. Hill", published in proceedings of 2000 SPIE conference, Orlando, FL



<sup>15</sup> Table available from E. Rosen of IDA with NVESD permission.

The columns in Figure 12 represent respectively: Column 1 – the UM file name, Column 2 – the number of edge points found by the Ellipse Detector that cause the maximum number of hits in the hit table, Column 3 – the maximum number of hits in a 3 by 3 by 5 region of the hit table, which is illustrated in Figure 5, and Column 4 the ground truth designation of mine (M) or clutter (C). The table entries have been sorted from highest to lowest value in Column 2, the Ellipse Detector decision metric used at the present time. When the decision threshold is set at greater than or equal to 26 for this metric, the Ellipse Detector has only one false alarm and one misdetection, giving  $P_D = 18/19 = 0.95$  at  $P_{FA} = 1/40 = 0.03$ .

Thus, the Ellipse Detector performance for the LDV is the same as the human performance for the blind test set. However, the Ellipse Detector used only coarse resolution output (about 4 inches resolution) while the human tests sometimes used finer resolution to confirm that certain images contained no mine. Also the Ellipse Detector made no use of contextual information that may have been perceived and exploited by the human operator.

The Ellipse Detector was also run on the PSI GPR blind test data set. The 48 entries of the GPR test set shown in Figure 13 contained the same mines and background as 48 of the 59 LDV images shown in Figure 12.

| TestSetApr99 Directory (Common LDV and GPR Mines and Clutter) |                  |          |          |           |          |                   |                  |          |          |           |          |
|---|------------------|----------|----------|-----------|----------|-------------------|------------------|----------|----------|-----------|----------|
| LDV/GPR Name  | True Class (IDA) | LDV (UM) | LDV (ED) | GPR (PSI) | GPR (ED) | LDV/GPR Name      | True Class (IDA) | LDV (UM) | LDV (ED) | GPR (PSI) | GPR (ED) |
| L03_002/t145b   | M15 (2-in)       | M        | M        | M         | M        | L03_028/s150b,a,c | BLANK            | C        | C        | C         | C        |
| L03_004/t125b   | VS2.2 (1-in)     | M        | M        |           |          | L04_022/s210b,a,c | BLANK            | C        | C        | C         | C        |
| L03_005/t115b   | EM12 (1-in)      | M        | M        |           |          | L03_011/s55b,a,c  | BLANK            | C        | C        | C         | C        |
| L04_021/t219b   | EM12 (2-in)      | M        | M        | M         | M        | L04_017/t259b     | BLANK            | C        | C        | C         | C        |
| L04_020/t229b   | VS2.2 (2-in)     | M        | M        | M         | M        | L03_006/t105b     | BLANK            | C        | C        | C         | C        |
| L04_006/t205b   | TMA4 (2-in)      | M        | M        | M         | M        | L04_008/s224b,a,c | BLANK            | C        | C        | C         | C        |
| L04_003/t175b   | VS2.2 (1-in)     | M        | M        | M         | M        | L04_002/t165b     | BLANK            | C        | C        | C         | C        |
| L03_017/t40b  | TMA4 (2-in)      | M        | M        | M         |          | L03_008/t85b      | BLANK            | C        | C        | C         | C        |
| L03_013/s35b,a  | VS1.6 (1-in)     | M        | M        | M         | M        | L04_023/s200b,a,c | BLANK            | C        | C        | C         |          |
| L04_025/s180b,c   | TM62P3 (2-in)    | M        | M        | M         | M        | L04_011/s254b,a,c | BLANK            | C        | C        | C         | C        |
| L03_022/s90b,a,c  | VS1.6 (3-in)     | M        | M        |           |          | L03_024/s110b,a,c | BLANK            | C        | C        | C         | C        |
| L03_027/s140b,c   | EM12 (1-in)      | M        | M        | M         | M        | L04_024/s190b,a,c | TMA4 (6-in)      |          |          |           | M        |
| L04_012/s264b,c   | VS2.2 (4-in)     | M        | M        | M         | M        | L04_001/s160b,a,c | BLANK            | C        | C        | C         | C        |
| L03_025/s120b   | M21 (3-in)       | M        | M        | M         | M        | L04_026/s170b,a,c | BLANK            | C        | C        | C         | C        |
| L04_013/s275b   | M15 (3-in)       | M        | M        | M         | M        | L04_005/t195b     | BLANK            | C        | C        | C         | C        |
| L03_009/t75b  | TM62M (6-in)     | M        | M        | M         | M        | L04_004/t185b     | BLANK            | C        | C        | C         | C        |
| L03_020/s70b,a,c  | BLANK            | C        | C        | C         | C        | L03_019/t60b      | BLANK            | C        | C        | C         | C        |
| L04_019/s239b,a,c   | BLANK            | C        | C        | C         | C        | L03_007/t95b      | BLANK            | C        | C        | C         | C        |
| L03_015/t20b  | BLANK            | C        | C        | C         | C        | L03_001B/t155b    | BLANK            | C        | C        | C         | C        |
| L04_015/t280b   | BLANK            | C        | C        | C         | C        | L04_014/s285b,a,c | BLANK            | C        | C        | C         | C        |
| L03_014/s25b,a,c  | BLANK            | C        | C        | C         | C        | L04_016/t270b     | BLANK            | C        | C        | C         | C        |
| L03_023/s100b,a,c   | BLANK            | C        | C        | C         | C        | L03_026/s130b,a,c | BLANK            | C        | C        | C         |          |
| L03_021/s80b,a,c  | BLANK            | C        | C        | C         | C        | L03_016/t30b      | BLANK            | C        | C        | C         | C        |
| L04_018/t249b   | BLANK            | C        | C        | C         | C        | L03_003/t135b     | BLANK            |          | C        |           | C        |

 denotes a misdetection,  denotes a false alarm

**Figure 13 Detection performance summary on Ellipse Detector and human decisions for the LDV and GPR**

Of the 48 entries in Figure 13, 17 are targets and 31 are clutter as indicated in Columns 2 and 8 where target type and depth are indicated and "BLANK" indicates clutter. The number of LDV edges found by the Ellipse Detector on the LDV images are used to sort the entries in Figure 13 as in Figure 12. Columns 1 and 7 give the UM file designation followed by the PSI file designation for the common mine and background in the blind test set.

Note that several GPR files can correspond to a single LDV file; hence the GPR designation s239b,a,c indicates three GPR files, corresponding to the single LDV file, L04\_019. When several GPR files exist, the Ellipse Detector decision is a mine, M, if any of the files produce a mine present decision. This procedure is currently a simple expedient that will be examined more thoroughly in our multilook fusion studies. Columns 3 through 6 and 9 through 12 indicate the decisions (M is mine and C is clutter) made by the procedure indicated in the column headers that represent, respectively, LDV (UM) - LDV human decision, LDV (ED) - Ellipse Detector LDV decision, GPR (PSI) – GPR human decision, and GPR (ED) - Ellipse Detector GPR decision.

The Ellipse Detector performance on the GPR test sets is  $P_D = 13/17 = 0.76$  at  $P_{FA} = 2/31 = 0.06$ . While this performance is somewhat less than the human GPR performance of  $P_D = 0.76$  at  $P_{FA} = 0.03$ , the difference

represents only one additional sample being called a false alarm. Given this GPR performance and the LDV performance of the Ellipse Detector, the Ellipse Detector appears to be performing as well as a human expert. Note that the Ellipse Detector makes faster decisions than an expert can make and is currently using only coarse sensor information. We are continuing to investigate further improvements to the Ellipse Detector itself, and we believe that it will be an important component to our ultimate robust mine detector.

## **6. SUMMARY AND CONCLUSIONS**

This paper presents the Signal Processing and Algorithm Development for Robust Mine Detection Program (SPAD) methodology, Ellipse Detector, and signal processing techniques applied to the mine detection task. The tools and techniques developed have focused on the robustness and multisensor requirements of the detection algorithm. The Ellipse Detector has been demonstrated to perform well on a variety of sensors. These sensors are acoustic, ground penetrating radar, and SAR. The SAR results used the Ellipse Detector, which is being developed for mine hunting, to detect adjacent vehicular targets.

Although these results are anecdotal for any single sensor due to the small number of images, the consistently good performance over all the sensors provides confidence that the Ellipse Detector is robust and effective. The ability of the Ellipse Detector to seamlessly fuse multichannel LDV images across frequency has also been demonstrated. This fusion allows the selection of the optimal frequency band for image enhancement and feature extraction.

The need for signal processing as a preprocessor to the Ellipse Detector has been shown for both the LDV and the GPR sensors. This signal processing is sensor dependent. The present results suggest that only relatively straightforward signal processing may be needed for the Ellipse Detector. In any case, the development and assessment of signal processing techniques is most effective when done in conjunction with the development of a specific detector such as the Ellipse Detector.

We have shown through an independently developed blind test data set that the Ellipse Detector performance is currently comparable to human expert performance on the LDV and GPR sensor output. The current Ellipse Detector uses only a few physical features. As the need arises, additional features will be extracted and exploited. This exploitation of new features will be done judiciously since the Ellipse Detector, itself, should be kept as robust and sensor independent as possible. As resources permit, the Ellipse Detector will be applied to images from other sensors, e.g., other GPR and IR sensors. During the next fiscal year, we will start making these algorithms adaptive.

The 3-year SPAD program is making considerable progress in its first year of work. For the remainder of this fiscal year, the focus is to quantify the Ellipse Detector in terms of receiver operating characteristic (ROC) curves for both the LDV and PSI GPR sensors and to develop a multisensor fusion algorithm for their outputs. The Ellipse Detector's ability to fuse PSI GPR depth images similar to LDV multichannel fusion will also be examined.